Nanoparticle assembly via the dewetting of patterned thin metal lines: Understanding the instability mechanisms

Lou Kondic
Department of Mathematical Sciences, Center for Applied Mathematics and Statistics, New Jersey Institute of Technology, Newark, New Jersey, USA

Javier A. Diez
Instituto de Física Arroyo Seco, Universidad Nacional del Centro de la Provincia de Buenos Aires, Pinto 399, 7000 Tandil, Argentina

Philip D. Rack, Yingfeng Guan, and Jason D. Fowlkes
Department of Materials Science and Engineering, The University of Tennessee, Knoxville, Tennessee 37996, USA and Oak Ridge National Laboratory, Oak Ridge, Tennessee 37831, USA

(Received 23 October 2008; revised manuscript received 9 December 2008; published 4 February 2009)

Nanosecond pulsed laser heating was used to control the assembly of spatially correlated nanoparticles from lithographically patterned pseudo-one-dimensional nickel lines. The evolution of the nickel line instabilities and nanoparticle formation with a correlated size and spacing was observed after a series of laser pulses. To understand the instabilities that direct the nanoparticle assembly, we have carried out nonlinear time-dependent simulations and linear stability analysis based on a simple hydrodynamic model. We find that the simulated time scales and length scales agree well with the experimental results. Interestingly, in both experiments and simulations, the instabilities associated with the line edge, and with the surface perturbation-driven mechanism, are found to result in similar particle sizes and spacings.

DOI: 10.1103/PhysRevE.79.026302 PACS number(s): 47.20.Dr, 81.16.Rf, 68.08.−p, 68.55.−a

I. INTRODUCTION

The synthesis and assembly of functional nanomaterials with unique properties is critical to realizing many of the overarching goals of nanotechnology. While top-down lithographic patterning has been successfully utilized in many micro- and nanoscale electronic, optical, biological, and mechanical applications, the future of nanoscale device architectures will likely require the confluence of both top-down and bottom-up self-assembly techniques. Recently, it has been shown that hydrodynamic instabilities induced by nanosecond laser pulses can be utilized to create two-dimensional arrays of spatially correlated nanoparticles [1–5]. Furthermore, capillary induced transport of lithographically patterned two- and three-dimensional features has been studied and suggests the possibility of a programmable self-assembly approach [6–9].

Studies on initial hole formation in films have shown that they are typically driven by nucleation at defect sites which are not spatially correlated, or via free surface instabilities where a critical wave vector is dynamically unstable thus yielding spatial correlation of the resultant particle size and spacing [1,4,10,11]. Once a hole is formed, the subsequent material transport is typically dominated by curvature induced surface diffusion when in the solid state [12,13], or by capillary forces if in the liquid state [3,4]. Recent works have considered additional effects that are of relevance to metal films irradiated by laser pulses, such as thermal effects and resulting Marangoni forces [4,14], and evaporative mass loss [15]. For the metal films of the thickness larger than few nanometers, it has been shown that a typical distance between the final patterns scales with H^2, where H is the film thickness. Additional Marangoni effects were considered as well, and it was shown that for Co and Fe films thicker than a certain critical length, these effects may lead to a decrease of the wavelength of maximum growth resulting from linear stability analysis (LSA), as the film thickness is increased.

While the dewetting characteristics of continuous thin films have been studied more extensively, patterned lines and shapes are also of practical importance. Chemically patterned surfaces have been used to investigate spatially confined wetting properties. For instance, Darhuber *et al.* [16] lithographically patterned a monolayer of octadecyltrichlorosilane (OTS) onto silicon oxide surfaces to pattern hydrophobic (OTS) and hydrophilic (silicon oxide) regions. Various glycerol volumes were applied to the patterned surfaces and the subsequent geometries were tested experimentally and compared to simulations. Gold nanoparticles have been oriented via solid state dewetting of gold films deposited onto inverted silicon pyramids [6]. Choi *et al.* [7] later patterned gold nanoparticles, and from the gold particles synthesized silicon nanowires from the gold nanoparticle array via a vapor-solid-liquid growth process. Habenicht *et al.* [8] recently investigated dewetting induced nanoparticle jumping which results from the dewetting front inertia of pulsed laser irradiated nanoscale gold triangles. Favazza *et al.* [5] carried out double-beam laser irradiation of Co films and found that repeated exposure lead to formation of nanowires of cylindrical shape which break up into nanoparticles characterized by a typical distance that scales as the square root of the cylinder thickness. Recently we have explored the dewetting characteristics and evolution of pulsed laser irradiated of patterned nickel circles, triangles, and squares [9]. The dynamics of the different vertices and edges were compared and correlated to the capillary driven dewetting dynamics.

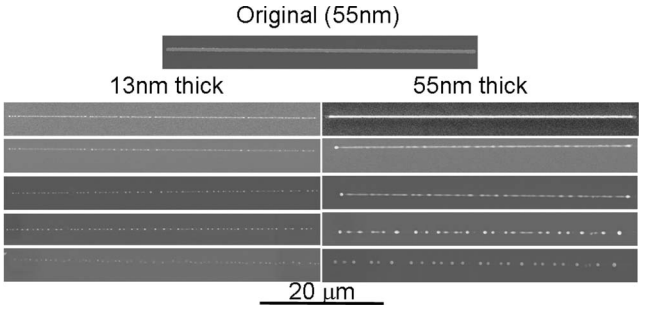

FIG. 1. SEM's of 50 μm long 420 nm wide and 13 nm (left) and 55 nm (right) thick Ni lines after one, two, three, five, and ten laser pulses progressing from top to bottom, respectively.

While hydrodynamic instabilities can be realized by conventional thermal processing, nanosecond (or shorter) pulsed laser heating offers nanosecond control of the liquid lifetimes, and therefore unique control of the material transport. Additionally, the ultrafast cooling rates achievable via laser induced heating can create materials far from equilibrium, which is an important scientific grand challenge [12]. Thus to realize the utility of nanosecond laser processing as a means to organize nonequilibrium nanoscale materials, in this paper we investigate the instabilities and subsequent materials transport of pseudo-one-dimensional nickel lines. One important difference compared to the previous works is that we consider lines of finite length, and discuss the instabilities that propagate from the ends (fronts) of the lines, in addition to surface-driven instabilities.

II. EXPERIMENT

Initially, Ni films (13 ± 2 nm and 55 ± 2 nm) were dc sputter deposited from a Ni foil (3 in. diameter, 30 W, 3 mTorr Ar sputtering gas) onto electron beam lithography patterned polymethylmethacrylate (or PMMA) coated (60 nm) silicon substrates. Ni lines 420 nm wide and 50 μm long were achieved by a conventional lift-off process. No attempt was made to remove the native silicon oxide film. Subsequently the 13 and 55 nm patterned lines were simultaneously laser treated with a series of 25 ns (full width at half maximum) 248 nm wavelength laser pulses with an energy density of 420 mJ/ cm^2, which was previously determined to be above the melting threshold of Ni [13]. The laser-induced liquid lifetime was simulated to be 25 and 40 ns per pulse for the 13 and 55 nm thick lines, respectively [17]. A total of ten laser pulses were applied to the lines, and to understand the dewetting evolution, scanning electron imaging was performed after pulses 1, 2, 3, 5, and 10.

Figure 1 is a series of scanning electron micrographs (SEM's) of the 13 nm thick (left) and 55 nm thick (right) Ni lines as a function of the laser pulse number. The most obvious observation in Fig. 1 is that the initially straight continuous lines evolve and transform into an array of nanoparticles whose size and spacing is a function of the original thickness. The first stage of evolution (not resolvable in Fig. 1) is a contraction of the 420 nm initial line width to an average width of 108 nm for the 13 nm line and 209 nm for the 55 nm line.

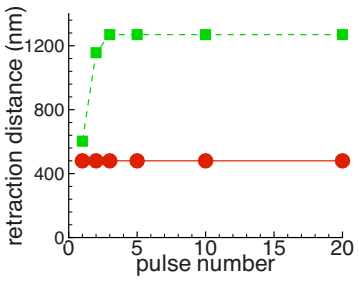

FIG. 2. (Color online) Experimental retraction distance as a function of pulse number for 13 nm (lower curve) and 55 nm (upper curve).

Figure 2 shows explicitly the retraction distance, defined as the distance between the initial line edge and the outer boundary of the edge particle. In this figure, we see that the transition into the ordered nanoparticle array occurs faster for the 13 nm line (by fifth pulse) relative to the 55 nm line (by tenth pulse). Furthermore, for the 55 nm lines we observe more clearly the "pearling" process by which the particle formation propagates from the edge.

Particle sizes were determined by thresholding the image contrast in the SEM images and performing a pixel counting routine; the spacings were determined by calculating the distance between the centroids of each pixel agglomeration. Figure 3 shows histograms of the particle size (a, b) and particle spacing (c, d) for the 13 nm (a, c) and 55 nm (b, d) lines. Using the histogram data and assuming the particles are hemispherical, the estimated volume reduction of the 13 nm line was 20% and was negligible for the 55 nm thick line. This is consistent with our previous results [13] and is attributed to silicide formation and some ablation. The volume reduction is intuitively more severe for the thinner film as the surface to volume ratio is larger.

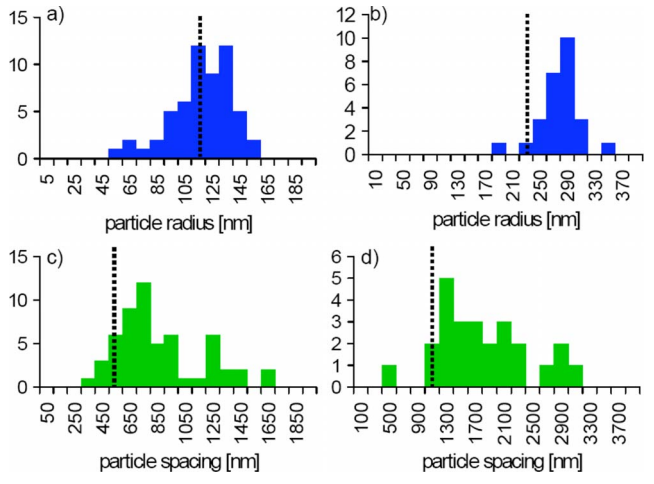

FIG. 3. (Color online) Histograms of the resultant particle size (a, b) and the particle spacing (c, d) of the 13 nm (a, c) and the 55 nm (b, d) Ni lines. The data were taken after fifth and tenth laser pulse for the 13 and 55 nm lines, respectively. The dotted lines show the predictions of the linear stability analysis discussed in the text.

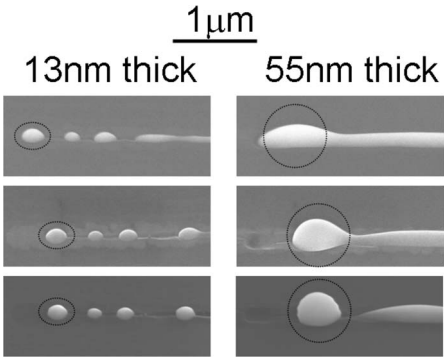

FIG. 4. Higher resolution and tilted (45°) SEM's of the left edge of the 13 nm (left) and 55 nm (right) Ni lines after one, two, and three laser pulses. For reference, the dashed circles show the edge particle.

Figure 4 shows tilted (45°) higher resolution images of the left edge of the Ni lines in Fig. 1, demonstrating the topology of the lines or particles. After the initial laser pulse the "rectangular" line transforms to a cylindrical shape which recesses slightly into the substrate. As evidenced in Fig. 4, the Ni line edge retracts as a consequence of the laser exposure. This figure clearly shows that after the first pulse, the 13 nm line has already broken up into several particles at the edge of the line, whereas the 55 nm line continues retracting and does not form the edge particle until the third laser pulse (viz. also Fig. 2). The retraction distance of the edge particle for the 13 nm line is 480 nm, whereas the 55 nm thick line retracts 1270 nm before the edge nanoparticle forms.

III. MODEL

Closer inspection of the images in Fig. 1 suggests that there are two separate phenomena responsible for nanoparticle formation: (i) instability induced by the finite size (edge instability), and (ii) instability of the body of the line itself. The latter one has been considered via various approaches in the past [5,18,19]. The instability due to finite size effects for liquid films has been considered recently [20], and an obvious question is whether the approach developed in that work applies to the current problem. For films it was found that the drop (particle in our case) spacing depended on the instability mechanism [20], the result related to the difference between spinodal and nucleation instabilities [1]. Whether this result applies to the lines considered here is of direct relevance since Fig. 1 suggests that both instability mechanisms are active and operate on similar time scales.

To quantify the discussion above, we list the assumptions which allow us to apply the formulation developed in [20], extended to the geometry considered here:

(i) the main part of the evolution occurs during the time when the line is in liquid phase [21];

(ii) the effect of volume reduction can be ignored;

(iii) liquid properties are constant in time—therefore melting and solidification are assumed to take place infinitely fast, and furthermore, Marangoni effects are neglected;

(iv) the metal-substrate interaction can be modeled using a disjoining pressure model with both conjoining and disjoining terms;

(v) lubrication approximation can be used despite large contact angles relevant to the experiment.

Under these assumptions, the following fouth order nonlinear partial differential equation for the line thickness $h(x,y,t)$ is obtained (given here in nondimensional form using the scales discussed below)

$$\frac{\partial h}{\partial t} + \nabla \cdot (h^3 \nabla \nabla^2 h) + \mathcal{K} \nabla \cdot [h^3 f' \nabla h] = 0. \qquad (1)$$

Here, (x,y) are the in-plane coordinates, with x pointing along the metallic line. Similar equations have been extensively used to analyze dewetting of thin liquid films (see, e.g., [10,22,23] and references therein). We note that more complete models including the thermal effects and Marangoni forces have been considered (e.g., [14,15]); here we are looking for a minimal model including the most relevant physics. In Eq. (1), the first term stands for viscous dissipation and the two other terms account for capillarity and liquid-solid interaction, respectively. Once the length scale ℓ is chosen, the corresponding time scale is $\tau = 3\mu\ell/\gamma$, where μ is the viscosity, and γ is the surface tension. We use $\ell = 1\ \mu$m, $\gamma = 1714$ dyn/cm, $\mu = 0.05$ g/cm s, giving $\tau = 8.75$ ns. Also, we have $\mathcal{K} = \kappa\ell/\gamma$ and $f' = df/dh$, where the function f enters through disjoining pressure defined by

$$\Pi(h) = \kappa f(h) = \kappa[(h_*/h)^n - (h_*/h)^m]. \qquad (2)$$

Here, κ (Hamaker constant) is defined by $\kappa = S/(\mathcal{M}\ell h_*)$, where $S = \gamma(1-\cos\theta)$ is the spreading parameter, θ is the contact angle, and $\mathcal{M} = (n-m)/[(m-1)(n-1)]$ (see [20] and note that in the present formulation h_* corresponds to *dimensionless* precursor film thickness). In Eq. (2), the first term represents liquid-solid repulsion, while the second one is attractive, leading to a stable film thickness $h = h_*$. Formation of such a film thickness (not observed within the experimental accuracy of the present experiments) may contribute to the observed volume loss; however, since the contribution of precursor to the total volume is small, we do not consider this effect in more detail. We use $n = 3$, $m = 2$, $\theta = 90°$ and note that this and similar models have been extensively used to model the interaction of liquid metal (e.g., [1]) and other liquid films (e.g., [10,22,24]) with solid substrates.

IV. RESULTS AND DISCUSSION

We consider the governing evolution equation (1) using linear stability analysis (LSA) and fully nonlinear time-dependent simulations. One important ingredient in both approaches is the thickness scale entering into the definition of Hamaker constant h_*, which can be related to the so-called precursor film. Since small values of h_* significantly slow down the simulations discussed in what follows, we use the larger value of h_* (typically $h_* = 10^{-3}$) and then confirm in select cases that the results depend very weakly on the exact value of h_*. Gravity is ignored due to nanometric line thickness. This model is applied to the line of initial profile as in the experiment, with smoothened boundaries. Since the nonlinear simulations are computationally expensive, we use

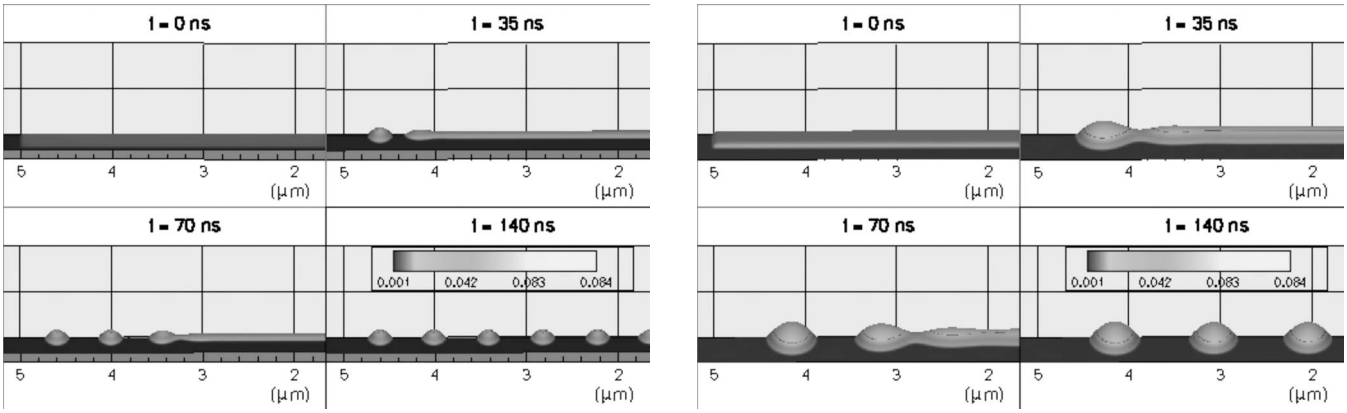

FIG. 5. The simulation results for the evolution of two considered line thicknesses. The legends show the thickness in μm.

them here for the purpose of demonstrating the main features of the instability development, and direct comparison to the experiment. LSA is then used to obtain more general conclusions regarding the issues such as the manner in which the final distance between the particles scales with the dimensions of the initial film.

A. Nonlinear simulations

Nonlinear simulations are performed using the finite-difference based method described in some detail elsewhere [25]; here we give a brief overview. The calculations are carried out in a rectangular computational domain defined by $0 \leqslant x \leqslant x_{max}$ and $0 \leqslant y \leqslant y_{max}$, which is divided into cells of size $\delta x \times \delta y$. Equation (1) is discretized in space using a central finite difference scheme. Time discretization is performed using implicit Crank-Nicolson scheme. We note that all the results presented in this paper are fully converged, as verified by grid refinement. We find that $\delta_x \leqslant 0.01$, $\delta_y \leqslant 0.0025$ is required for full convergence. Larger gradients of the solution required smaller grid size in the y direction. We use the symmetry of the problem and simulate only a quarter of the whole rivulet.

Nonlinear simulations show that the initial profile quickly contracts to semicylindrical shape, in agreement with the experiments. Figure 5 shows the breakup that occurs from the edges for the two considered line thicknesses. The retraction distances are 400 and 800 nm for the 13 and 55 nm lines, respectively, close to the experimental results (see Fig. 2). The time scale on which detachment of the first particle occurs for 13 nm is $\tilde{t} \approx 25$ ns ≈ 1 pulse; experiments also observe edge breakup at this time scale. For 55 nm, this detachment occurs at $\tilde{t} \approx 50$ ns, therefore faster compared to the experiment, where three pulses are needed for the first particles to form. Considering, however, that the material parameters (viscosity, surface tension) are not well known, and that the model itself is rather simple, we find this agreement very encouraging.

The fact that a reasonable agreement between nonlinear simulations and experiments is achieved using lubrication model for a problem characterized by large contact angle suggests that the details of contact line physics are not crucial in determining the evolution. Furthermore, we note that our model ignores the Marangoni forces due to temperature gradients in the film thickness which may inhibit instability growth and contribute to the longer time scales observed in experiments [14].

Remark 1. We note that in principle further coarsening of the drops may be expected due to the presence of precursor film [26]; however, here we concentrate only on the short time scale and therefore do not consider this effect in more detail.

Remark 2. We do not carry out fully nonlinear simulations with additional surface perturbations, since we have shown previously that the influence of these perturbations can be considered more efficiently by linear stability analysis [20]. This is the topic of the following section.

B. Linear stability analysis

The linear stability analysis (LSA) is used to discuss the breakup that occurs all along the line length (therefore it does not account for the finite length effects). It is carried out by expanding around the x-independent solution, $h_0(y)$, of Eq. (1):

$$h(x,y,t) = h_0(y) + \epsilon g(y) \exp(\sigma t + ikx), \tag{3}$$

where $\epsilon \ll 1$, $g(y)$ is the amplitude of the perturbation, $k = 2\pi/\lambda$ is the wave number, and λ is the wavelength. The base solution, $h_0(y)$, is discussed in some detail in Appendix B of [20]. In the present context, $h_0(y)$ is chosen in a way that the enclosed area $\mathcal{A}$ is equal to the initial line cross section, i.e.,

$$\mathcal{A} = \int_{-w/2}^{w/2} [h_0(y) - h_*] dy = \frac{WH}{\ell^2},$$

where H is the initial line thickness, and $W = \ell w$ is its width. By replacing Eq. (3) into Eq. (1), we obtain to $O(\epsilon)$ the eigenvalue problem:

$$\mathcal{L} g = -\sigma g,$$

where $\mathcal{L}$ is the linear operator defined by

$$\mathcal{L}g = c_4(y)g_{yyyy} + c_3(y)g_{yyy} + c_2(y)g_{yy} + c_1(y)g_y + c_0(y)g, \tag{4}$$

where the coefficients $c_i(y)$ $(i=0,\ldots,4)$ are defined by

$$c_4(y) = h_0^3,$$

$$c_3(y) = 3h_0^2 h_0',$$

$$c_2(y) = -(2k^2 - \mathcal{K}f')h_0^3, \tag{5}$$

$$c_1(y) = -h_0^2[3(k^2 - \mathcal{K}f') - 2h_0\mathcal{K}f'']h_0',$$

$$c_0(y) = c_{0,2}h_0^2 + c_{0,3}h_0^3, \tag{6}$$

where $c_{0,j}$ $(j=2,3)$ is given by:

$$c_{0,2}(y) = 3h_0'^2\mathcal{K}f'',$$

$$c_{0,3}(y) = k^2(k^2 - \mathcal{K}f') - \mathcal{K}f''(p + \mathcal{K}f) + h_0'^2\mathcal{K}f'''.$$

Here, p is the dimensionless pressure (in units of γ/ℓ) inside the rivulet, which is related with enclosed area $\mathcal{A}$ (see [20]). This pressure is the integration constant needed to determine $h_0(y)$ from the solution of the steady one-dimensional version of Eq. (1). Then, the eigenvalue problem is solved numerically, with the main goal of answering the following questions:

(i) What is the size of initial perturbation which leads to growth on the time scale comparable to the experimental one? Does this size make physical sense?

(ii) What is the particle spacing predicted by LSA? Does this spacing correspond to the one resulting from the edge-driven instability?

(iii) What are the predictions of LSA regarding scaling of the distance between the particles with the initial line thickness?

Figure 6 shows the results for the dimensional wavelength of maximum growth, $\tilde{\lambda}_m$, which can be compared with the particle spacing (all the results are now given in dimensional units in order to facilitate comparison to experiments). We obtain $\tilde{\lambda}_m \approx 560$ nm for the 13 nm line, and 1150 nm for the 55 nm line, in good agreement with experiment, viz. Figs. 3(c) and 3(d).

The time scale of instability growth is estimated as

$$\tilde{t}_s = \frac{1}{\tilde{\sigma}} \ln\left(\frac{H}{\epsilon\ell}\right),$$

where $\tilde{\sigma}$ is the dimensional growth rate of $\tilde{\lambda}_m$ [alternatively, one could use $\max(h_0(y))\ell$ instead of H for the purpose of this estimate, with similar results]. Using fixed $\epsilon = 10^{-4}$ (corresponding to 0.1 nm), LSA gives $\tilde{t}_s \approx 45$ ns and ≈ 115 ns for the 13 nm and 55 nm lines, respectively, corresponding to the liquid lifetimes resulting from two (13 nm) and three (55 nm) pulses. The comparison of relevant time scales between the results of LSA and nonlinear simulations, viz. Fig. 5, shows that for the 13 nm line one expects surface perturbation-driven mechanisms to dominate, while for the 55 nm line, both mechanisms operate on similar time scales, as also seen in the experiments. Additional results show that $\tilde{\lambda}_m$ and $\tilde{t}_s$ depend only weakly on the value of Hamaker's constant.

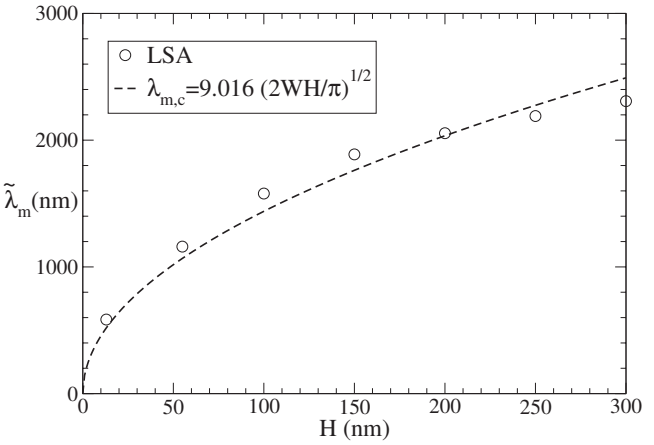

FIG. 6. Dimensional wavelength, $\tilde{\lambda}_m$ of maximum growth from LSA vs line thickness H. The first two data points correspond to $H=13$ and 55 nm, and we use $W=420$ nm. The dashed line shows the prediction for a capillary instability of a free standing liquid jet (Rayleigh-Plateau theory).

By comparing the LSA results for $\tilde{\lambda}_m$ with the distance between the particles resulting from edge-driven instability shown in Fig. 5, we see that they are very close. This behavior differs from the breakup of semi-infinite liquid films, where one may expect disparate length scales resulting from the two instability mechanisms [20]. Therefore, for a line breakup, we find that the particle spacing does not depend on the mechanism leading to their formation. This is one of the main results of this work.

The second important difference between the instabilities of films and lines is scaling of the distance D between the particles with the line thickness. As mentioned in the Introduction, the scaling expected for liquid metal films in the spinodal regime, assuming that Marangoni effects can be ignored, is that $D \propto H^2$. However, the experiments and simulations (viz. Figs. 4 and 5) show that the evolution is different here, since the initial line quickly reaches semicylindrical shape, and the instability occurs only aftwerwards. If now for a moment one ignores liquid metal–solid substrate interaction, and considers stability of a free-standing liquid jet, an application of classical Rayleigh-Plateau result gives $D \propto \sqrt{H}$, since the use of conservation of mass gives that the radius of the cylinder is approximately given by $R_c \approx \sqrt{2HW/\pi}$.

Figure 6 shows the LSA results for several additional values of line thickness. In this figure we see that the LSA results closely follow the square root scaling specified above, which is also in agreement with the recently reported experiments [5]. Figure 6 also shows the approximate (dimensional) wavelength of maximum growth [27],

$$\tilde{\lambda}_{m,c} = 9.016R_c,$$

expected from capillary instability for a free standing liquid jet (Rayleigh-Plateau instability). The agreement between the two results suggests that, at least for the considered problem, Rayleigh-Plateau result gives a very good prediction for the distance between the particles. The growth rate of the mode $\tilde{\lambda}_{m,c}$ predicted by Rayleigh theory is

$$\tilde{\sigma}_{m,c} \approx 0.3433 \sqrt{\frac{\gamma}{\rho R_c^3}},$$

where ρ is the liquid density (we use $\rho = 8.9\ \mathrm{g/cm^3}$). For example, for $H = 55$ nm, the predicted value is $1/\tilde{\sigma}_{m,c} \approx 8.85$ ns, which is of the same order of magnitude as the growth rate predicted by LSA. Therefore we conjecture that, at least for this problem, the influence of liquid metal–solid surface interaction on the instability development is rather weak, since both the distance between the particles and the time scale of growth are consistent with the capillary instability of a free-standing liquid jet.

Regarding particle size, we note that it can also be predicted by LSA if one considers that a particle is hemispherical and its mass is equal to that of a line of length $\tilde{\lambda}_m$ (therefore ignoring the volume loss observed in the experiments). Then, the particle radius is given by $R_p = [3\tilde{\lambda}_m WH/(2\pi)]^{1/3}$. This calculation yields 113 and 230 nm for $H = 13$ and 55 nm, respectively, in good agreement with the experimental data reported in Figs. 3(a) and 3(b). In more general terms, using the scaling $\tilde{\lambda}_m \propto \sqrt{H}$ discussed above, and assuming conservation of mass, one finds $R/\tilde{\lambda}_m = \mathrm{const}$, as also discussed in [5]. Therefore LSA gives clear predictions for both particle size and the distance between the particles.

V. CONCLUSION

In this work, we have considered the details of the instability mechanism leading to breakup of metal lines repeatedly irradiated by laser pulses. We find that the main features of instability development can be understood based on a relatively simple hydrodynamic model. The model includes the capillary forces as well as the liquid-solid interaction via disjoining pressure approach. We find reasonably good agreement between the experiments carried out using laser irradiated Ni lines, linear stability analysis, and fully nonlinear time-dependent simulations. The simulations include the end effects due to finite length of the metal lines. In contrast to liquid films, we find that the breakup caused by the end effects leads to similar distance between the particles as the breakup caused by surface instabilities. However, the time scales of relevance to these two instability processes may be different. For the considered configurations, we find that for thinner lines, the surface instability is expected to dominate (a line breaks up all along its length in the same time), while for thicker lines, the end-driven instability plays an important role.

We expect that the fact that a relatively simple hydrodynamic model can explain the main features of the considered experiments will lead to future experimental and theoretical works demonstrating enhanced spatial control. Future work will also explore the resultant structure and properties of the assembled nanomaterials.

ACKNOWLEDGMENTS

P.D.R. and J.D.F. acknowledge that a portion of this work was performed at Oak Ridge National Laboratory's Center for Nanophase Materials Sciences which is sponsored by the Scientific User Facilities Division, Office of Basic Energy Sciences, U.S. Department of Energy. J.A.D. acknowledges support from Consejo Nacional de Investigaciones Científicas y Técnicas de la República Argentina (CONICET) and from Agencia Nacional de Promoción Científica y Tecnológica (ANPCyT) through Grant No. PICT 2498/06.

[1] S. Herminghaus, K. Jacobs, K. Mecke, J. Bischof, A. Fery, M. Ibn-Elhaj, and S. Schlagowski, Science **282**, 916 (1998).
[2] C. Favazza, R. Kalyanaraman, and R. Sureshkumar, Nanotechnology **17**, 4229 (2006).
[3] J. Bischof, D. Scherer, S. Herminghaus, and P. Leiderer, Phys. Rev. Lett. **77**, 1536 (1996).
[4] J. Trice, D. Thomas, C. Favazza, R. Sureshkumar, and R. Kalyanaraman, Phys. Rev. B **75**, 235439 (2007).
[5] C. Favazza, J. Trice, R. Kalyanaraman, and R. Sureshkumar, Appl. Phys. Lett. **91**, 043105 (2007).
[6] A. L. Giermann and C. V. Thompson, Appl. Phys. Lett. **86**, 121903 (2005).
[7] W. K. Choi, T. H. Liew, H. G. Chew, F. Zheng, C. V. Thompson, Y. Wang, M. H. Hong, X. D. Wang, L. Li, and J. Yun, Small **4**, 330 (2008).
[8] A. Habenicht, M. Olapinski, F. Burmeister, P. Leiderer, and J. Boneberg, Science **309**, 2043 (2005).
[9] P. Rack, Y. Guan, J. Fowlkes, A. Melechko, and M. Simpson, Appl. Phys. Lett. **92**, 223108 (2008).
[10] J. Becker, G. Grün, R. Seemann, H. Mantz, K. Jacobs, K. R. Mecke, and R. Blossey, Nature Mater. **2**, 59 (2003).
[11] F. Brochard-Wyart and C. Redon, Langmuir **8**, 2324 (1992).
[12] G. Fleming and M. Ratner, Phys. Today **61**(7), 28 (2008).
[13] Y. Guan, R. Pearce, A. Melechko, D. K. Hensley, M. Simpson, and P. Rack, Nanotechnology **19**, 235604 (2008).
[14] J. Trice, C. Favazza, D. Thomas, H. Garcia, R. Kalyanaraman, and R. Sureshkumar, Phys. Rev. Lett. **101**, 017802 (2008).
[15] V. Ajaev and D. Willis, Phys. Fluids **15**, 3144 (2003).
[16] A. A. Darhuber, S. M. Troian, S. M. Miller, and S. Wagner, J. Appl. Phys. **87**, 7768 (2000).
[17] A. J. Pedraza, Y. F. Guan, J. D. Fowlkes, and D. A. Smith, J. Vac. Sci. Technol. B **22**, 2823 (2004).
[18] S. H. Davis, J. Fluid Mech. **98**, 225 (1980).
[19] L. Yang and G. M. Homsy, Phys. Fluids **19**, 044101 (2007).
[20] J. Diez and L. Kondic, Phys. Fluids **19**, 072107 (2007).
[21] C. Favazza, R. Kalyanaraman, and R. Sureshkumar, J. Appl. Phys. **102**, 104308 (2007).
[22] U. Thiele, M. G. Velarde, and K. Neuffer, Phys. Rev. Lett. **87**,

016104 (2001).
[23] A. Oron, S. H. Davis, and S. G. Bankoff, Rev. Mod. Phys. **69**, 931 (1997).
[24] K. B. Glasner and T. P. Witelski, Phys. Rev. E **67**, 016302 (2003).
[25] J. Diez and L. Kondic, J. Comput. Phys. **183**, 274 (2002).
[26] L. M. Pismen and Y. Pomeau, Phys. Fluids **16**, 2604 (2004).
[27] P. G. Drazin and W. H. Reid, *Hydrodynamic Stability* (Cambridge University Press, Cambridge, England, 1991).